# Thermal and Flame Retardant Properties of Ethylene-Vinyl Acetate Copolymer/Modified Multiwalled Carbon Nanotube Composites

**Lichun Wang,[1,2] Ping Kai Jiang[1,2]**

[1]*School of Chemistry and Chemical Engineering, Shanghai Jiao Tong University, Shanghai 200240, People's Republic of China*
[2]*Shanghai Key Lab of Electric Insulation and Thermal Aging, Shanghai 200240, People's Republic of China*

Received 6 May 2010; accepted 27 June 2010
DOI 10.1002/app.33028
Published online 21 September 2010 in Wiley Online Library (wileyonlinelibrary.com).

**ABSTRACT:** The synthesized flame retardant 9,10-dihydro-9-oxa-10-phosphaphanthrene-10-oxide/vinyl methyl dimethoxysilane (DV) was used to modify multiwalled carbon nanotubes (MWNTs). The results of FTIR, $^1$H-NMR, and TGA measurements show that DV has been covalently grafted onto the surfaces of MWNTs, and the MWNTs-*g*-DV is obtained successfully. Transmission electron microscopy images show that a core-shell nanostructure appears with MWNTs as the core and the DV thin layers as the shell, and the modified MWNTs with DV can achieve better dispersion than unmodified MWNTs in EVM matrix. Thermogravimetric analysis and cone calorimeter tests indicate that the thermal stability and flame retardant are improved for the presence of the MWNTs in EVM matrix. Moreover, the improvement is more evident for EVM/MWNTs-*g*-DV composite compared to unmodified MWNTs-based composite, which can be attributed to the better dispersion of the DV-modified MWNTs and to the chemical structure of the combustion residue. © 2010 Wiley Periodicals, Inc. J Appl Polym Sci 119: 2974–2983, 2011

**Key words:** ethylene-vinyl acetate copolymer; multiwalled carbon nanotube; flame retardant; composites

## INTRODUCTION

Carbon nanotubes (CNTs) have attracted more and more attention since 1991.[1] A panel of phenomena and properties associated with CNTs caused by their special combination of dimension, structure, and topology has been investigated over the past number of years.[2–5] In recent years, many reports indicate that CNTs offer another candidate as a flame retardant additive.[6–13] However, the insolubility and tending to aggregate limit the manipulation and processing of CNTs and result in their nonuniform dispersion in common solvents and polymer matrices.

Ethylene vinyl acetate (EVA) copolymer is widely used in the cable industry. As the VA content increases, the copolymer presents increasing polarity but lower crystallization, and therefore different mechanical behavior. The increasing polarity with increasing VA content is apparently useful in imparting a high degree of polymer-filler surface interaction, which is very important for polymer composites with high loading fillings in practical applications. Ethylene-vinyl acetate copolymer rubber (EVM) (VA% content is generally 40–80%) is suitable for use as halogen-free flame retardant wire and cable materials because of its good properties. It is required to introduce fire retardants alumina trihydrate (ATH) or magnesium dihydroxide (MDH) in high content to avoid fire hazards and reduce flammability. However, this high mineral loading results in a worsening of the mechanical performance of the materials.[14] Recently, the researches about the use of tiny amounts of CNTs as flame retardant systems have been a great interest in the EVA copolymer matrix.[15–17]

Organophosphorus compounds have proved to be good flame retardants (FRs) for polymeric materials. The cyclic phosphorus group, 9,10-dihydro-9-oxa-10-phosphaphenanthrene-10-oxide (DOPO), has received notable attention in research owing to its attractive properties. DOPO and its derivatives are widely incorporated into polymers for improving the polymers' FR properties and thermal stability.[18–22] In a previous report,[23] a novel flame retardant intermediates of silicane oligomer containing phosphorous, 9,10-dihydro-9-oxa-10-phosphaphanthrene-10-oxide/vinyl methyl dimethoxysilane (DOPO-VMDMS), has been successfully synthesized and used in PC/ABS alloys. In the previous works, it was found that the residual char was 41.8% in air, while it was only 25.2% in nitrogen for the synthesized flame retardant DV in TGA tests. This interesting result indicated that the

*Correspondence to:* P. K. Jiang (pkjiang@sjtu.edu.cn).

silicon containing compounds degrade to generate silicon dioxide in air that could not be oxidized further and left in the carbon layer. The thermal stability of the char layer was further improved, and more residual char was observed in air than in nitrogen at high temperature, which was commonly very important to improve the flame retardant property. This study aims to modify multiwalled carbon nanotubes (MWNTs) with DOPO-VMDMS and prepare according EVM/MWNTs composites. It is anticipated that the functionalizing of MWNTs can improve the dispersion of MWNTs and promote the thermal stability and flame retardancy of EVM/MWNTs composites.

## EXPERIMENTAL

### Materials

A commercial cable grade ethylene-*co*-vinyl acetate copolymer (EVM) rubber (Levaprene 500HV) was kindly supplied by Bayer, Germany. The vinyl acetate content is 50 wt %, the Mooney viscosity ($ML_{1+4}$ (100°C)) is 27 ± 4, MFI (g/10 min) is lower than 5 and the density is 1.00 g/cm$^3$. DOPO was purchased from Shandong Mingshan Chemical, China. Vinylmethyldimethoxy silane (VMDMS; Brand: SILQUEST A2171) was acquired from GE silicones. Two types of MWNTs (pristine MWNTs and functionalized MWNTs with hydroxyl group: MWNTs-OH) with the same aspect ratios (outer diameter: 10–20 nm, inner diameter: 5–10 nm, length: 10–30 μm) synthesized by chemical vapor deposition were purchased from Chengdu Organic Chemistry, Chinese Academy of Science. Potassium hydroxide (KOH), chloroform ($CHCl_3$), and acetone were acquired from Shanghai Chemical, China.

### Synthesis of 9, 10-dihydro-9-oxa-10-phosphaphanthrene-10-oxide/vinyl methyl dimethoxysilane[23]

A total of 200 mL $CHCl_3$, 27 g (0.125 mol) DOPO and 16.5 g (0.125 mol) VMDMS were added to a 500-mL three-necked round bottom flask fitted with a stirrer under nitrogen conditions. The temperature was kept to the reflux temperature of $CHCl_3$ (62°C) for 12 h. After this, the water solution of KOH (5%, wt) was added as a catalyst for 8 h to obtain an oligomer product (DOPO-VMDMS). Finally, the solvent was removed by the vacuum-pumping. The reaction equation is shown in Figure 1(a).

### The modification of MWNTs-OH with DOPO-VMDMS

The mixture of 10.0 g MWNTs-OH and 150 mL anhydrous $CHCl_3$ were added into a 250-mL flask and dispersed in ultrasonic bath for 2 h. Then the $CHCl_3$ solution of DOPO-VMDMS was injected into the reaction system with a reflux condenser and refluxed at 63°C

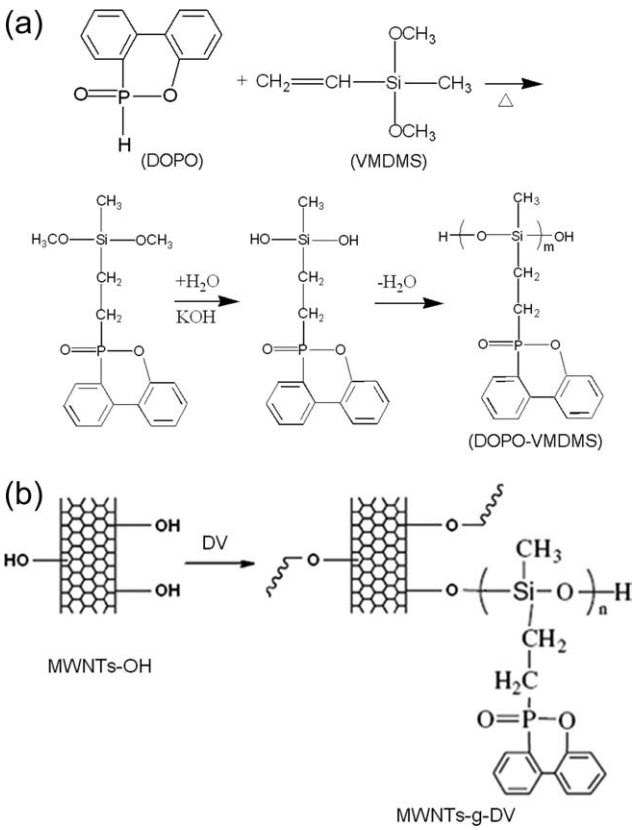


**Figure 1** The synthesis route of DV (a) and MWNTs-*g*-DV (b).

under $N_2$ atmosphere for 24 h. The resultant was ultrasonically washed with $CHCl_3$ and acetone to remove any unreacted silane oligomer. The DOPO-VMDMS modified MWNTs-OH (MWNTs-*g*-DV) were obtained and dried under vacuum. The FTIR, $^1$H-NMR spectra, and TEM were used to characterize the organically modified MWNTs (MWNTs-*g*-DV). The grafted DV content of MWNTs-*g*-DV was determined by TGA. The synthesis route for MWNTs-*g*-DV was shown in Figure 1(b).

### Preparation of EVM/MWNT composites

EVM pallets were dried at 45°C in a vacuum for 3 h before processing to remove moisture. Then the EVM/MWNTs and EVM/MWNTs-*g*-DV nanocomposites containing 1.0, 2.0 phr of MWNTs or 2.0 phr of MWNTs-*g*-DV were prepared via melt compounding at 110°C in Thermo Haake Rheomix with a screw speed of 60 rpm, and the mixing time was 12 min for each sample. The obtained mixtures were subsequently pressed into sheets of suitable thickness to obtain samples for further measurements.

### Measurements and characterization

FTIR and $^1$H-NMR spectroscopy

The FTIR spectra of MWNTs, DV, and MWNTs-*g*-DV were recorded with KBr powder by using a

Perkin–Elmer Paragon 1000 instrument. The structure of DV and MWNTs-*g*-DV were characterized by hydrogen nuclear magnetic resonance ($^1$H-NMR), which were performed on an Mercuryplus 400 (300 MHz) NMR spectrometer with DMSO-$d_6$ as a solvent.

### Transmission electron microscopy

Morphology of MWNTs, MWNTs-*g*-DV, and their dispersion in the EVM matrix were observed with a JEM 2100 transmission electron microscope (TEM) at an accelerating voltage of 200 kV. For TEM observation, MWNTs and MWNTs-*g*-DV were dissolved in chloroform, and the solution was dropped onto a copper grid and then dried under vacuum. The samples of EVM/MWNTs and EVM/MWNTs-*g*-DV composites were cooled at −80°C and then microtomed with a diamond knife to give sections with a nominal thickness of 50−150 nm.

### Optical microscopy

An XP-203 optical microscopy (OM), product of Changfang Optical Instrument, Shanghai, China, with charge-coupled device (CCD) camera was used to study the dispersion of MWNTs and MWNTs-*g*-DV in EVM matrix.

### Thermogravimetric analysis

The thermogravimetric analysis (TGA) was performed with a Perkin–Elmer Q 50 thermal analyzer at a heating rate of 20°C/min under the nitrogen atmosphere, and the temperature ranged from room temperature to 800°C.

### Cone calorimeter test

Cone calorimeter uses a truncated conical heater element to irradiate test specimens at heat fluxes from 10 to 100 kW/m$^2$, thereby simulating a range of fire intensities. The technique is a small scale fire test, but it has been shown to provide data that correlate well with those from full-scale fire tests.[24] Cone calorimeter tests were carried out in duplicate, using a 35-kW/m$^2$ incident heat flux, following the procedures indicated in the ISO 5660 standard with a FTT cone calorimeter.[25] Each specimen, of dimensions 100 × 100 × 3 mm$^3$, was wrapped in aluminum foil and placed on a mineral fiber blanket with the surface level with the holder, such that only the upper face was exposed to the radiant heater. The edge guard was used with all specimens, as was the recommended standard retaining grid to prevent excessive intumescence. The experimental error rate from the cone calorimeter test was about ±5%. The cone calorimeter technique provides detailed information about ignition behavior, heat release, and smoke evolution during sustained combustion and some key parameters that are correlated well with real fire.[26]

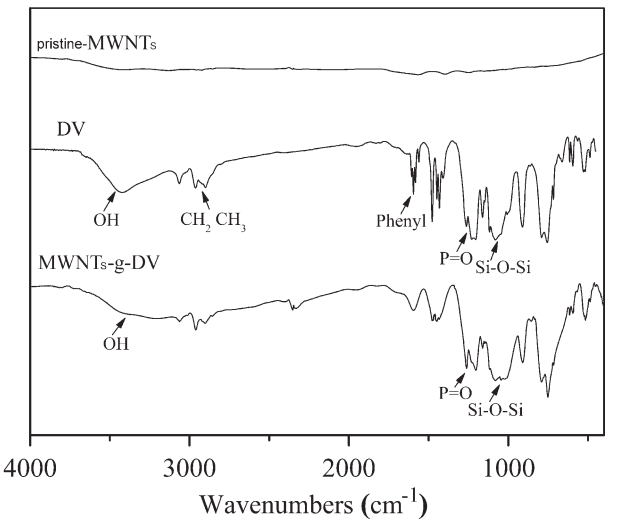


**Figure 2** FTIR spectra of MWNTs, DV, and MWNTs-*g*-DV.

### Microstructure analyses by SEM

Scanning electron microscopic (SEM) analyses for the morphology of EVM/MWNTs composites residues after combustion in cone calorimeter were made using a field emission scanning electron microscopy (FE-SEM, JEOL JEM-4701). The gold-coated samples to avoid accumulation of charges were analyzed at an accelerating voltage of 5.0 kV.

## RESULTS AND DISCUSSION

### Characterization of MWNTs-*g*-DV

Figure 2 shows the infrared spectra of the synthesized flame retardant DV and MWNTs-*g*-DV. In the FTIR spectrum of DV, the absorption peaks at 3421 (Si—OH), 3064 (C—H in phenyl group), 2800–3000 ($CH_2$, $CH_3$), 1595 (phenyl group), 1477 (P-phenyl), 1410 (P—$CH_2$— of aliphatic), 1206 (P=O), 1004–1117 (Si—O—Si) are found. Comparing with the FTIR spectrum of DV, it can be found that the characteristic peaks of hydroxyl groups in DV become weaker and the similar characteristic peaks appears from the spectrum of MWNTs-*g*-DV, demonstrating that the hydroxyl groups in DV have reacted with hydroxyl groups on the surface of MWNTs. Figure 3 shows the $^1$H-NMR spectra of DV and MWNTs-*g*-DV. The peaks of $^1$H-NMR ($d_6$-DMSO, ppm): −0.4 to 0.1 (Si—$CH_3$), 0.6 (C—$CH_2$—Si), 1.8–1.9 (—$CH_2$—P), 7.1–8.6 (benzene ring) were found in $^1$H-NMR of both DV and MWNTs-*g*-DV, while the characteristic peak

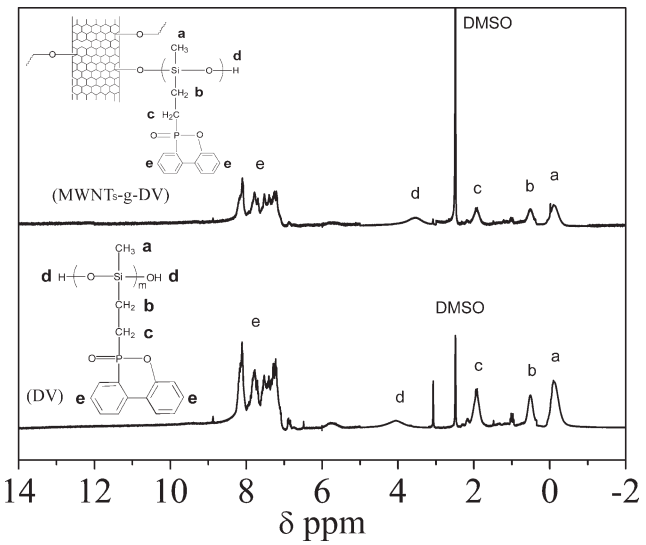


**Figure 3** $^1$H-NMR spectra of DV and MWNTs-*g*-DV in DMSO-$d_6$.

of 3.4 (Si—OH) in DV has shifted to 4.0 (Si—OH) in MWNTs-*g*-DV. The results of FTIR and $^1$H-NMR clearly indicated that DV has been attached to the external surface of MWNTs.

Measurements of TEM images can provide further direct evidence for the coatings of DV onto MWNTs. Thus, the MWNTs and MWNTs-*g*-DV were analyzed by TEM, and the results are shown in Figure 4. Figure 4(a) displays a typical TEM image of pristine MWNTs, showing a very smooth and clean surface for all the MWNTs. The tubes possess uniform inner and outer diameters of about 5–10 nm and 10–20 nm in average along their length, respectively. However, the functionalization of MWNTs with DV significantly alters the surface roughness of the MWNTs surface, with an evident increase in the diameter of the MWNTs. In addition, the core-shell structure with the DV layer as the shell and MWNTs crystal sheet as the core are clearly discerned from MWNTs-*g*-DV, and the thickness of the DV shell is about 6–10 nm in average shown in Figure 4(b). Undoubtedly, DV chains have been immobilized onto the surfaces of MWNTs.

The relative amounts of grafted DV in the MWNTs-*g*-DV can be determined by TGA through the thermal decomposition of DV because DV have a lower decomposition temperature than MWNTs. Figure 5 shows the TGA curves of pristine MWNTs, DV, and MWNTs-*g*-DV under $N_2$ atmosphere. Obviously, pristine MWNTs have good thermal stability under $N_2$ atmosphere. When the temperature is increased up to 800°C, there is no evident decomposition in pristine MWNTs and about 96 wt % residues are left. The synthesized flame retardant of DV is an excellent carbonization agent and 24 wt % residue remains after thermal degradation at 800°C. For MWNTs-*g*-DV, 57 wt % char is left at the end of decomposition in this test. Considering that the mutual influence on thermal degradation between DV and MWNTs is possible, the grafting degree of DV is only approximate but not accurate. Therefore, the TGA results can be applied to estimate the relative amounts of the grafted DV onto the convex walls of MWNTs. The difference in the weight loss between pristine MWNTs, DV, and MWNTs-*g*-DV can be calculated and shows that the DV amount is about 54 wt % in MWNTs-*g*-DV.

### The dispersion and morphology of MWNTs and MWNTs-*g*-DV in EVM matrix

The dispersion and morphology of MWNTs and MWNTs-*g*-DV in EVM matrix can be observed by the optical micrographs (OM) and the TEM images. Figure 6(a,b) shows the optical micrographs of EVM/MWNTs (2.0 phr) and EVM/MWNTs-*g*-DV (2.0 phr) composites, respectively. There are no evident agglomerations of the MWNTs-*g*-DV in Figure

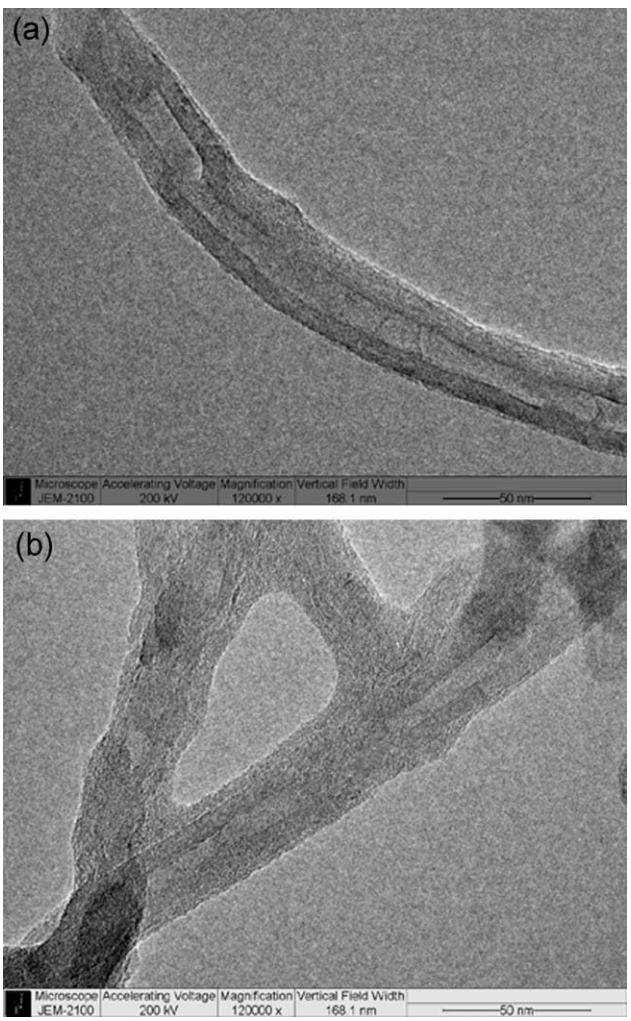


**Figure 4** TEM images of MWNTs (a) and MWNTs-*g*-DV (b).

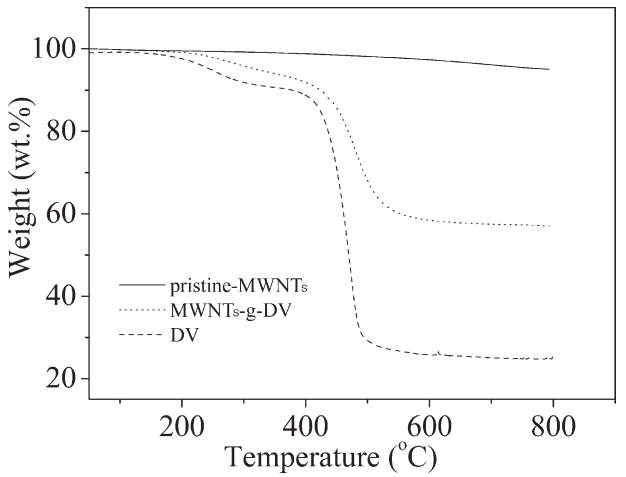


**Figure 5** TG curves versus temperature for MWNTs, DV, and MWNTs-*g*-DV under $N_2$ atmosphere.

6(b), while many black spots, which are attributed to MWNTs agglomerates, appear in Figure 6(a). This indicates that the MWNTs-*g*-DV is uniformly dispersed in the EVM matrix at the 100 μm scale. Figure 6(c,d) shows the TEM images of EVM/MWNTs (2.0 phr) and EVM/MWNTs-*g*-DV (2.0 phr) composites, respectively. It can be seen that the DV-modified MWNTs have been disordered and homogeneously dispersed throughout the EVM matrix in Figure 6(d) contrary to the unmodified MWNTs in Figure 6(c), for which very large MWNTs aggregates are still visible in the higher magnification images. Combining the aforementioned OM and TEM observation, it can be concluded that the MWNT-*g*-DV presents better dispersion in EVM matrix, either from submicrometer scale or from microscopic view. This significant change in the quality of MWNTs dispersion is due to the destruction of the native MWNT aggregates, which are thermodynamically stabilized by numerous π-π electronic interactions between the MWNTs; these π-π electronic interactions are still present in the EVM matrix.[27] Indeed, the functionality of MWNTs with the synthesized flame retardant DV, allows the MWNTs' external

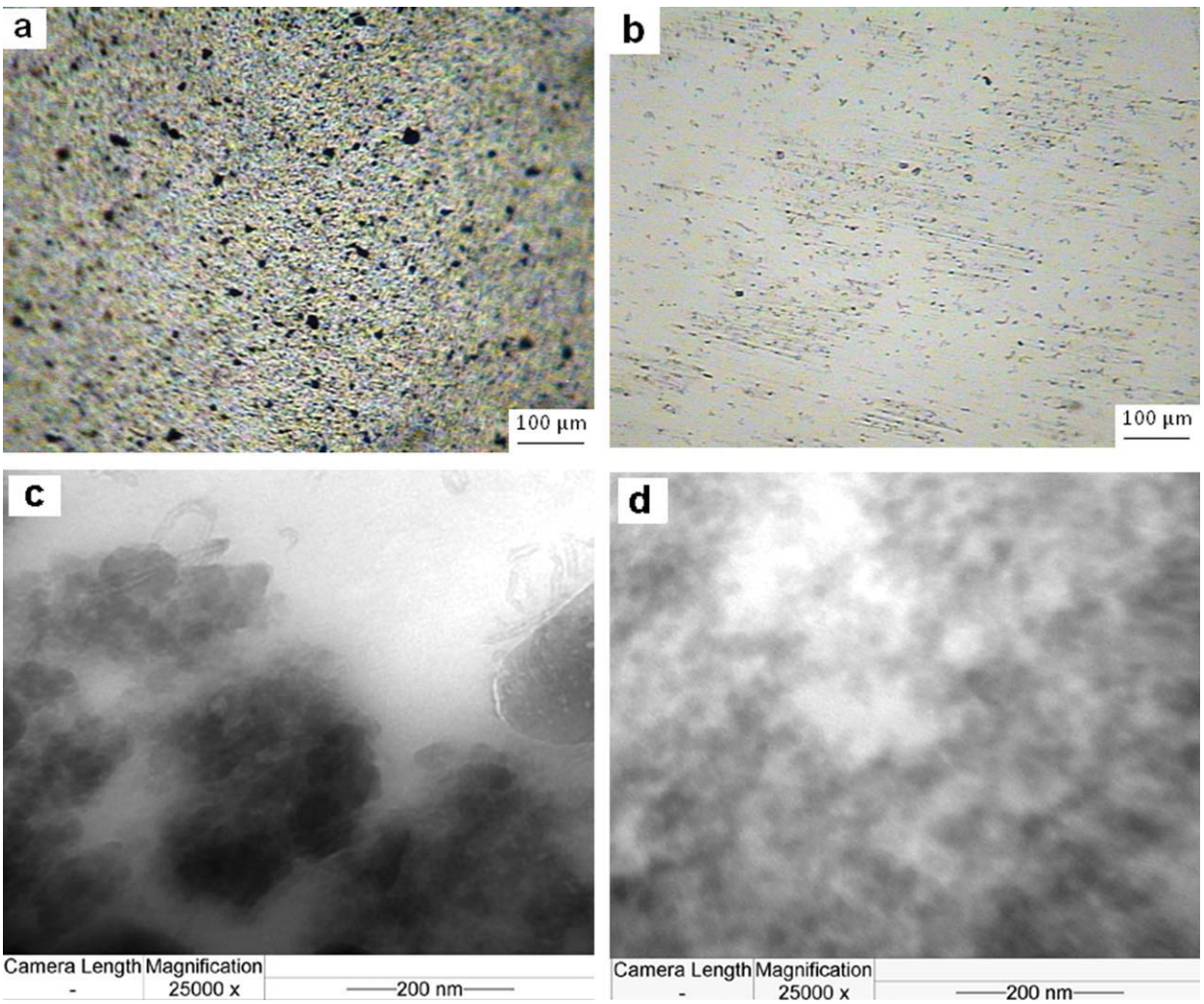


**Figure 6** Dispersions and morphologies of MWNTs and MWNTs-*g*-DV in EVM matrix: Optical micrographs of (a) EVM/MWNTs (2.0 phr); (b) EVM/MWNTs-*g*-DV (2.0 phr) composites and TEM images of (c) EVM/MWNTs (2.0 phr); (d) EVM/MWNTs-*g*-DV (2.0 phr) composites. [Color figure can be viewed in the online issue, which is available at wileyonlinelibrary.com]

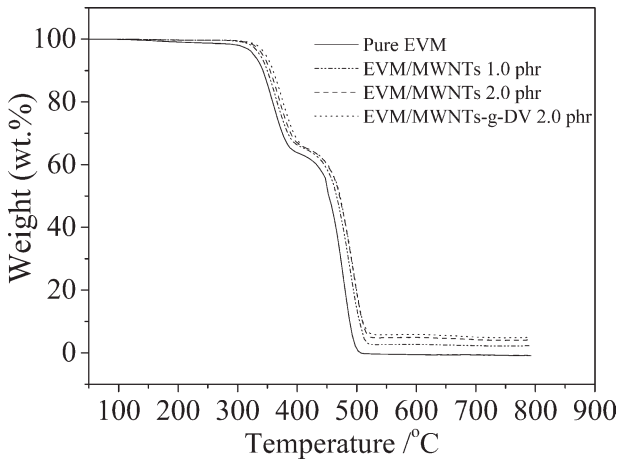


**Figure 7** TGA curves versus temperature or virgin EVM and the according flame retardant composites.

walls to be wrapped with a thin layer of DV, which impedes the π-π electronic interactions and accordingly promotes the formation of individual MWNTs that easily disperse in EVM matrix.

### Thermal stability of EVM/MWNTs and EVM/MWNTs-*g*-DV composites

The fire performance of materials is closely associated with the thermal degradation of materials. TGA is one of the commonly used techniques for the rapid evaluation of the thermal stability of different flame retardant materials, and it indicates the decomposition of polymers at various temperatures. Figure 7 presents the thermogravimetric (TG) curves of virgin EVM and the filled EVM composites with the two types of MWNTs under nitrogen atmosphere. It can be found that the thermodegradation of EVM copolymer takes place in two steps. The first step is considered to involve the deacetylation in the range of 300–380°C with the production of gaseous acetic acid and the formation of carbon–carbon double bonds along the polymer backbone. The onset temperature of the two filled EVM composites increases in varying degrees as the loading of MWNTs. This delay in weight loss is most probably due to the two reasons. The first is that the volatilization rate of acetic acid is limited, and a more thermally stable char is formed because of the higher viscosity of the composites in the melt state and the labyrinth effect of the interconnected fillers; the second may is that the limit of the molecular chains' movement arising from the network formation in the presence of MWNTs has modified the thermal behavior of EVM matrix. The second step of the thermal degradation is due to the volatilization of the residual polymer at temperatures between 380 and 500°C. After thermal degradation at 800°C, the residue increases (from 0.6 to 2.3, 4.2, and 5.1%) for the EVM/MWNTs (1.0 phr), EVM/MWNTs (2.0 phr), and EVM/MWNTs-*g*-DV (2.0 phr) composites as the loading of MWNTs. These indicate that the thermal stability of EVM matrix has been evidently improved for the presence of the carbon nanotubes as shown in Figure 7. Also, the better dispersion state of MWNTs is closely correlated to obtain better thermal stability for EVM/MWNTs composites.

### Flammability of EVM/MWNTs and EVM/MWNTs-*g*-DV composites

Cone calorimeter test based on the oxygen consumption principle has been widely used to evaluate the flammability characteristics of materials. Although cone calorimeter test is a small-scale test, the obtained results have been found to correlate well with those obtained from a large-scale fire test and can be used to predict the combustion behavior of materials in a real fire.[28–32] For instance, the heat release rate (HRR) is a very important parameter and can be used to express the intensity of a fire. A highly flame retardant system normally shows a low HRR value. In this research, cone calorimeter experimental results at a flux of 35 kW/m$^2$ are shown in Table I and Figures 8–11. It can be seen that the peak of heat release rate (PHRR) decreases from 836 kW/m$^2$ to 553 and 462 kW/m$^2$ as the loading of unmodified MWNTs increases, and the reduction in PHRR was nearly 34 and 45% for the EVM/MWNTs (1.0 phr) and EVM/MWNTs (2.0 phr) composites, respectively. Meanwhile, the reduction in PHRR for EVM/MWNTs-*g*-DV (2.0 phr) composites (47%) is more evident than EVM/MWNTs (2.0 phr) composites (45%). The reduction of HRR values was accompanied by a pronounced prolongation of burning time with a flat curve, while it presents very sharp and short HRR curve for pure EVM as shown in Figures 8 and 9.

**TABLE I**
**Cone Calorimeter Results of Unfilled EVM and Flame Retardant Composites**

| Formulation | EVM | EVM/ MWNTs 1.0 phr | EVM/ MWNTs 2.0 phr | EVM/ MWNTs-*g*-DV 2.0 phr |
|---|---|---|---|---|
| TTI (s) | 53 | 68 | 67 | 91 |
| PHRR (kW/m$^2$) | 836 | 553 | 462 | 441 |
| AHRR (kW/m$^2$) | 416 | 292 | 273 | 264 |
| THR (MJ/m$^2$) | 101 | 93 | 87 | 83 |
| FPI (m$^2$ s/kW) | 0.063 | 0.123 | 0.145 | 0.206 |
| AEHC (MJ/kg) | 33.2 | 28.6 | 26.4 | 25.7 |
| Residues (%) | 1.5 | 2.9 | 4.7 | 7.0 |

TTI: time to ignition; PHRR: peak of heat release rate, expressing the intensity of a fire; AHRR: average HRR within the front 200 s from heat radiation; FPI: fire performance index, the ratio of TTI and PHRR; AEHC: average effective heat of combustion.

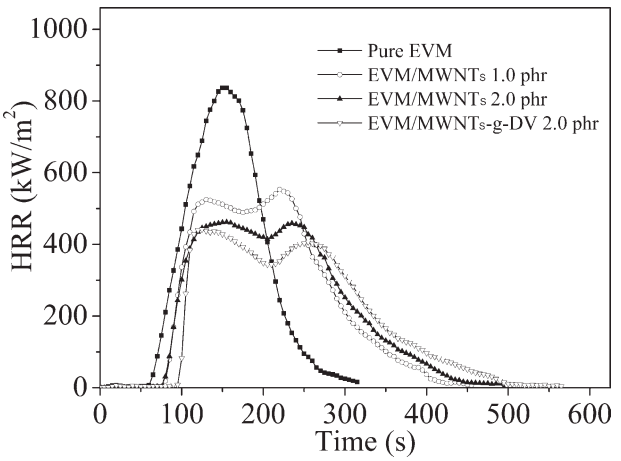


**Figure 8** HRRs versus burning time for virgin EVM and the according flame retardant composites.

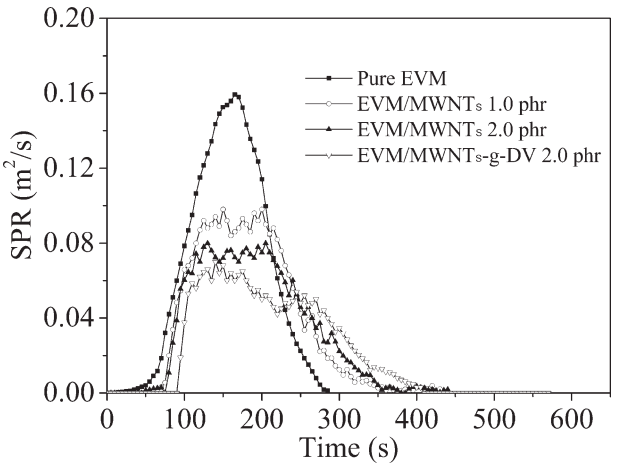


**Figure 10** SPRs versus burning time for virgin EVM and the according flame retardant composites.

The mass loss rate (MLR) curves [Fig. 9(a)] present a similar change with HRR curves. It can also be found that the residue mass after combustion increases due to the loadings of MWNTs and MWNTs-*g*-DV shown in Figure 9(b), which can be observed directly from the residual photographs after the cone calorimeter tests shown in Figure 11. The pure EVM matrix has been burnt out [Fig. 11(a)] and all the aluminum foil become visual, whereas the other samples for the MWNTs-based EVM composites remain more or less residues [Fig. 11(b–d)] and incumbent nearly or completely on the aluminum foil. An interesting effect of the modification of the MWNTs by the synthesized Si-P containing flame retardant DV has been observed on the cohesion of the combustion residues. It can be found that it presents a fragile and cracked char after combustion for the EVM/MWNTs (2.0 phr) material [Fig. 11(c)], whereas the MWNTs-*g*-DV-based composite with the same loading (2.0 phr) gives rise to a cohesive and uniform carbonaceous residue [Fig. 11(d)]. This better cohesion of the combustion residue of the composite based on MWNTs-*g*-DV could be explained by the more uniformly dispersion of modified MWNTs and the introduction of silicon with the charring ability from DV.

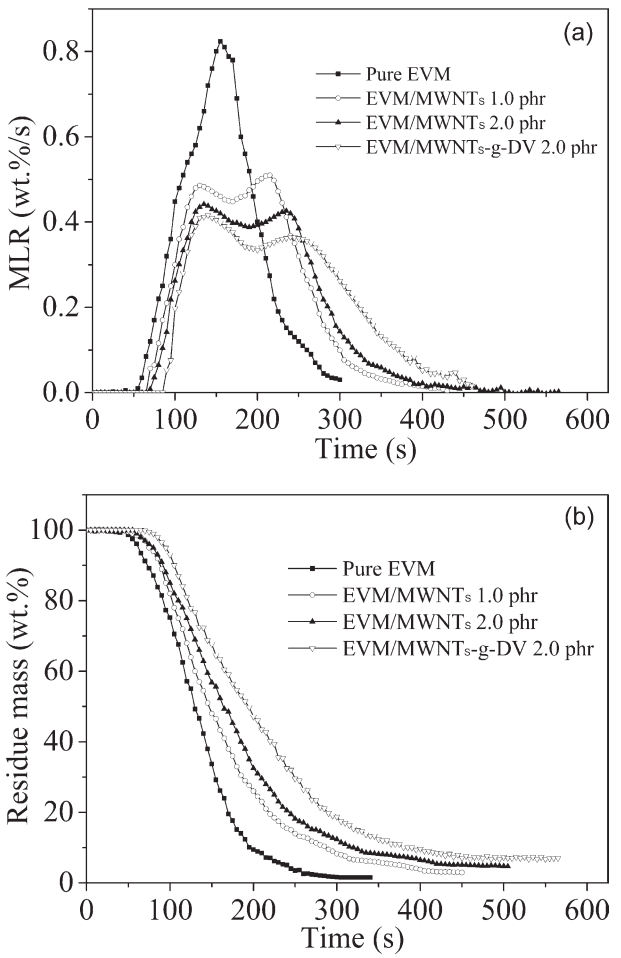


**Figure 9** MLRs (a) and residue mass (b) versus burning time for virgin EVM and the according flame retardant composites.

During the combustion in cone calorimeter, very strong bubbling and heavily melting was observed for the virgin EVM, whereas the EVM/MWNTs and EVM/MWNTs-*g*-DV composites did not show any bubbling, which may be probably due to the much higher melt viscosity compared to the unfilled EVM. Such an increase in melt viscosity is clearly due to the presence of the long CNTs in EVM matrix. This seems to confirm our explanation for the delay in the first degradation step recorded during TGA analysis and the increases of time to ignition (TTI) is shown in Table I. It can be seen (Table I) that the TTI increases (from 53 to 67, 68, and 91 s, respectively) for the EVM/MWNTs (1.0 phr), EVM/MWNTs (2.0 phr), and EVM/MWNTs-*g*-DV (2.0 phr) composites, which could be explained by the enhancement of thermal stability as recorded during

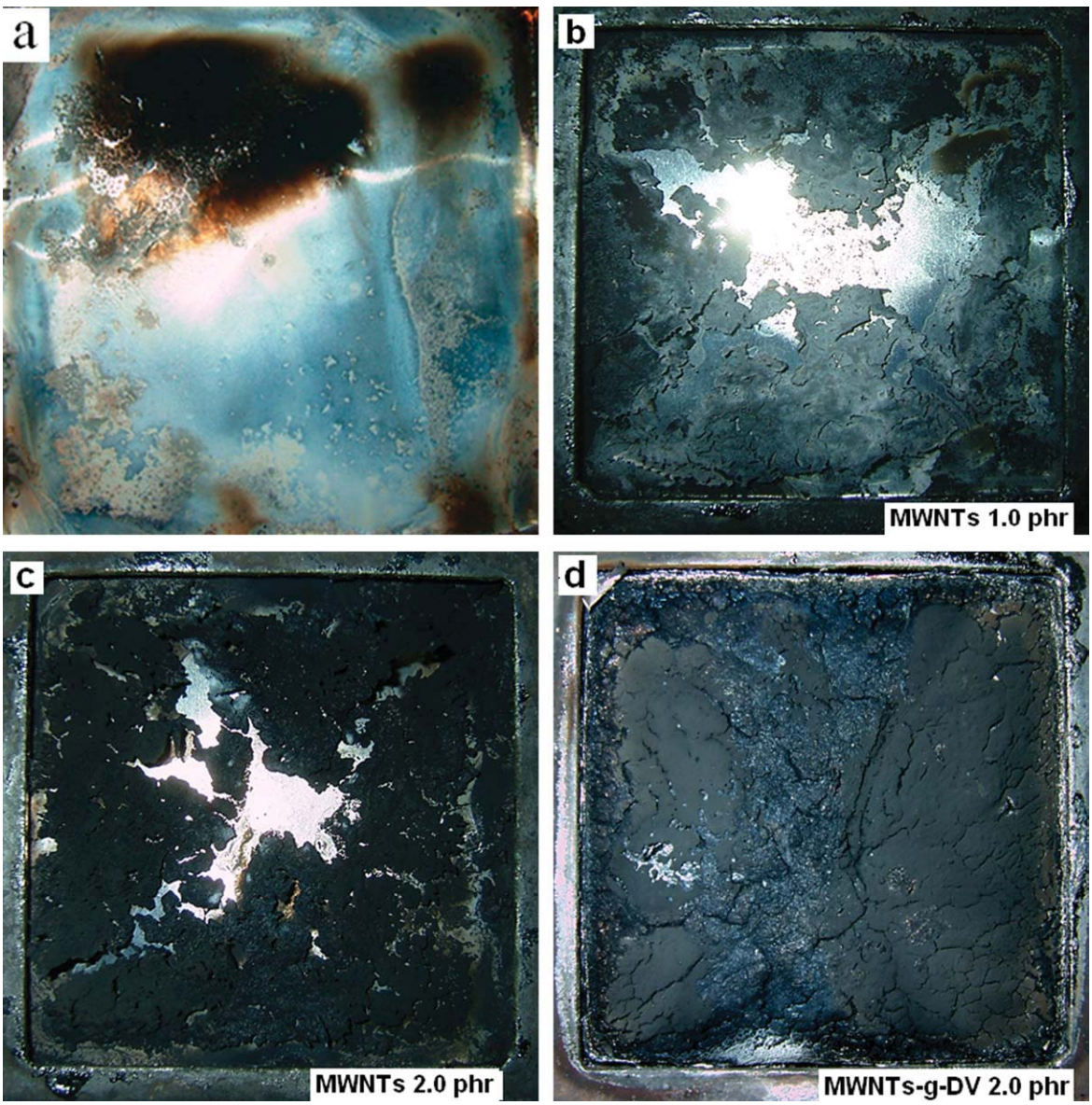


**Figure 11** Residual photographs of the samples after combustion: (a) virgin EVM; (b) EVM/MWNTs 1.0 phr; (c) EVM/MWNTs 2.0 phr; (d) EVM/MWNTs-*g*-DV 2.0 phr. [Color figure can be viewed in the online issue, which is available at wileyonlinelibrary.com]

TGA and the improvement of thermal conductivity for the filled EVM samples. Another important parameter in fire is fire performance index (FPI), which is the principal basis in designing a fleeing time for firemen. The longer the FPI is, the more chance for people to escape from fire. It is recognized that FPI is one of the most important parameters in real fire.[22–26] From Table I, it can be seen that the FPI increases to 0.123, 0.145, and 0.206 $m^2$ s/kW, respectively, for the EVM/MWNTs (1.0 phr), EVM/MWNTs (2.0 phr), and EVM/MWNTs-g-DV (2.0 phr) composites from 0.063 $m^2$ s/kW of virgin EVM. This is very important to increase the probability of escape and decrease the casualty in real fire. On the other hand, evaluation of the fire performance often involves quantifying smoke generation at the rate of smoke production (SPR). Figure 10 shows the SPR curves versus burning time for virgin EVM, EVM/MWNTs, and EVM/MWNTs-*g*-DV composites. It can be found that the SPR curves become flat and the peak SPR (PSPR) values decrease for both of the filled EVM composites compared to virgin EVM matrix; and the reduction is more evident for MWNTs-*g*-DV-based EVM composites than MWNTs-based EVM composites with the same loadings (2.0 phr). This may be the better cohesion of the combustion residues and the better catalysis of charring arising from the better dispersion of modified MWNTs.

To confirm the above explanation further, the microstructures of the combustion residues were observed and compared for EVM/MWNTs (2.0 phr) and EVM/MWNTs-*g*-DV (2.0 phr) composites

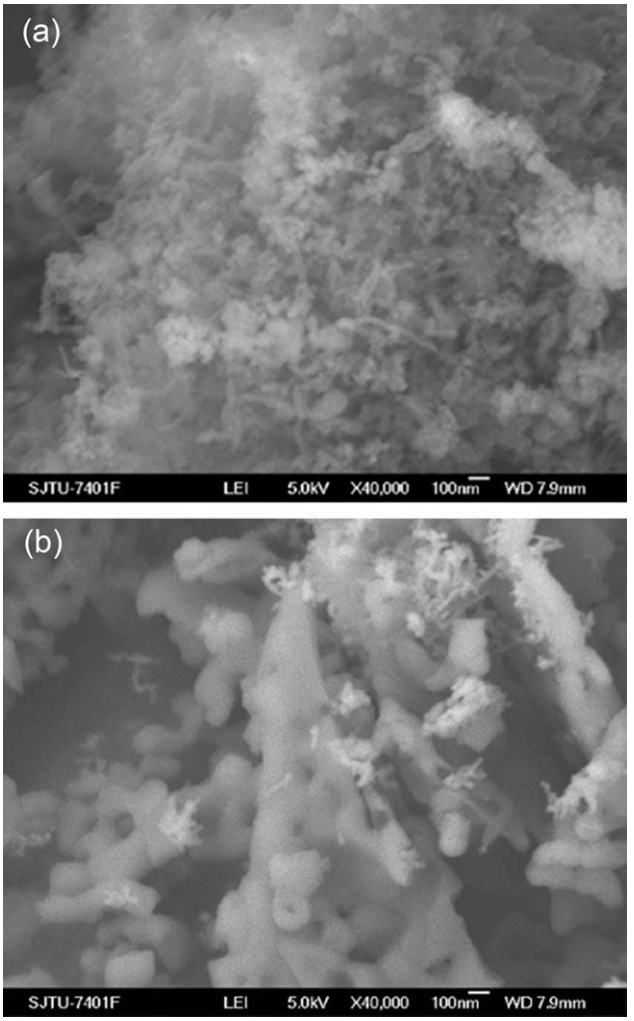


**Figure 12** The residual microstructure analysis after combustion for the samples of EVM/MWNTs 2.0 phr (a) and EVM/MWNTs-g-DV 2.0 phr (b).

by SEM and TEM. Figure 12 shows the SEM images of the residues after combustion for EVM/MWNTs (2.0 phr) and EVM/MWNTs-g-DV (2.0 phr) composites. It can be seen that the unmodified MWNTs almost maintain the original appearance of CNTs [Fig. 12(a)] and show a similar network structure consisting of bundled conglomeration after combustion. However, the network formed by the char of MWNTs-*g*-DV-based EVM composites is more compact, and some carbonaceous residues are cohesive on the surface of the MWNTs residue is shown in Figure 12(b). This can be observed more clearly from the TEM image of the residues after combustion for EVM/MWNTs-*g*-DV (2.0 phr) composites as shown in Figure 13. Much char with irregular shape wrapping the MWNTs residue is left after combustion for MWNTs-*g*-DV-based composite, and this is the most direct evidence for the effect of the modification of the MWNTs by DV on the cohesion of the combustion residues and carbonaceous residues.

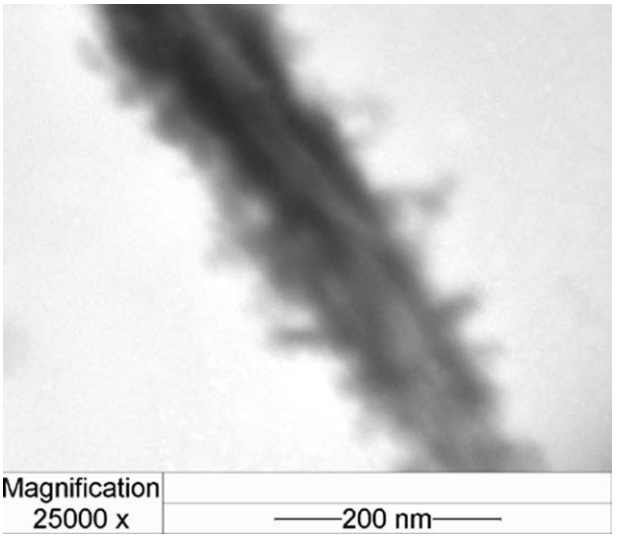


**Figure 13** TEM images of the residue for the sample of EVM/MWNTs-*g*-DV 2.0 phr after combustion.

## CONCLUSIONS

The MWNTs has been modified by the synthesized flame retardant DV and the MWNTs-*g*-DV was obtained successfully, which is confirmed by the evidence from the results of FTIR, $^1$H-NMR, and TGA measurements. A core-shell nanostructure with MWNTs as the core and the DV thin layers as the shell are observed by TEM images. The according EVM/MWNTs and EVM/MWNTs-*g*-DV composites have been prepared by the melting method. TEM images show that the modified MWNTs with DV can achieve better dispersion than unmodified MWNTs in EVM matrix. The presence of the MWNTs improves the thermal stability of the polymer matrix: the onset temperature and residue mass of the two filled EVM composites increases due to the loading of MWNTs as observed by TGA. As determined by cone calorimeter testing, some important parameters are influenced by adding MWNTs or modified MWNTs to EVM: the PHRR, THR, AHRR, MLR, SPR, and AEHC decreases; the TTI, FPI and residual mass increases for the EVM/MWNTs and EVM/MWNTs-*g*-DV composites compared to neat EVM. Compared to unmodified MWNTs-based composite, the reduction of the HRR is slightly improved; the TTI and FPI are evidently enhanced; the distribution and cohesion of the combustion residue is largely improved for EVM/MWNTs-*g*-DV composite. This phenomenon can be attributed to the better dispersion of the DV-modified MWNTs and to the chemical structure of the combustion residue.

## References

1. Iijima, S. Nature 1991, 354, 56.
2. Tasis, D.; Tagmatarchis, N.; Bianco, A.; Prato, M. Chem Rev 2006, 106, 1105.

3. Gao, C. Macromol Rapid Commun 2006, 27, 841.
4. Kuila, B. K.; Malik, S.; Batabyal, S. K.; Nandi, A. K. Macromolecules 2007, 40, 278.
5. Misra, A.; Greer, J. R.; Daraio, C. Adv Mater 2009, 21, 334.
6. Peeterbroeck, S.; Laoutid, F.; Taulemesse, J. M.; Monteverde, T.; Lopez-Cuesta, J. M.; Nagy, J. B.; Alexandre, M.; Dubois, P. Adv Funct Mater 2007, 17, 2787.
7. Kashiwagi, T.; Du, F. M.; Douglas, J. F.; Winey, K. I.; Harris, R. H.; Shields, J. R. Nat Mater 2005, 4, 928.
8. Yamamoto, G.; Omori, M.; Hashida, T.; Kimura, H. Nanotechnology 2008, 19, 315708.
9. Beyer, G. Fire Mater 2005, 29, 61.
10. Kashiwagi, T.; Grulke, E.; Hilding, J.; Harris, R.; Awad, W.; Douglas, J. Macromol Rapid Commun 2002, 23, 761.
11. Gao, F. G.; Beyer, G.; Yuan, Q. C. Polym Degrad Stab 2005, 89, 559.
12. Tang, T.; Chen, X. C.; Chen, H.; Meng, X. Y.; Jiang, Z. W.; Bi, W. G. Chem Mater 2005, 17, 2799.
13. Sarno, M.; Gorrasi, G.; Sannino, D.; Sorrentino, A.; Ciambelli, P.; Vittoria, V. Macromol Rapid Commun 2004, 25, 1963.
14. Gheysari, D.; Behjat, A. Eur Polym J 2002, 38, 1087.
15. Peeterbroeck, S.; Laoutid, F.; Swoboda, B.; Lopez-Cuesta, J. M.; Moreau, N.; Nagy, J. B.; Alexandre, M.; Dubois, P. Macromol Rapid Commun 2007, 28, 260.
16. Beyer, G. Fire Mater 2002, 26, 291.
17. Kashiwagi, T.; Du, F. M.; Winey, K. I.; Groth, K. A.; Shields, J. R.; Bellayer, S. P.; Kim, H.; Douglas, J. F. Polymer 2005, 46, 471.
18. Schartel, B.; Braun, U.; Balabanovich, A. I.; Artner, J.; Ciesielski, M.; Doring, M.; Perez, R. M.; Sandler, J. K. W.; Altstadt, V. Eur Polym J 2008, 44, 704.
19. Perez, R. M.; Sandler, J. K. W.; Altstadt, V.; Hoffmann, T.; Pospiech, D.; Ciesielski, M.; Doring, M.; Braun, U.; Knoll, U.; Schartel, B. J Mater Sci 2006, 41, 4981.
20. Zhong, H. F.; Wu, D.; Wei, P.; Jiang, P. K.; Li, Q.; Hao, J. W. J Mater Sci 2007, 42, 10106.
21. Lin, C. H. Polymer 2004, 45, 7911.
22. Lin, C. H.; Hwang, T. Y.; Taso, Y. R.; Lin, T. L. Macromol Chem Phys 2007, 208, 2628.
23. Zhong, H. F.; Wei, P.; Jiang, P. K.; Wang, G. L. Fire Mater 2007, 31, 411.
24. Hirschler, M. M.; Piansay, T. Fire Mater 2007, 31, 373.
25. International Organization for Standardization. Reaction to fire tests – heat release, smoke production and mass loss rate – Part 1: Heat release rate (cone calorimeter method), ISO 5660–1: 2002; International Organization for Standardization: Geneva, Switzerland.
26. Marney, D. C. O.; Russell, L. J.; Mann, R. Fire Mater 2008, 32, 357.
27. Jeon, J. H.; Lim, J. H.; Kim, K. M. Polymer 2009, 50, 4488.
28. Digges, K. H.; Gann, R. G.; Grayson, S. J.; Hirschler, M. M.; Lyon, R. E.; Purser, D. A.; Quintiere, J. G.; Stephenson, R. R.; Tewarson, A. Fire Mater 2008, 32, 249.
29. Morgan, A. B.; Gagliardi, N. A.; Price, W. A.; Galaska, M. L. Fire Mater 2009, 33, 323.
30. Fu, X.; Zhang, C.; Liu, T.; Liang, R.; Wang, B. Nanotechnology 2010, 21, 235701.
31. Chow, W. K.; Han, S. S.; Zeng, W. R. Cell Polym 2010, 29, 73.
32. Zanetti, M.; Kashiwagi, T.; Falqui, L.; Camino, G. Chem Mater 2002, 14, 881.